

# ICSV14

Cairns • Australia  
9-12 July, 2007



## THE ROLE OF THE INFLOW MOMENTUM THICKNESS IN SUBSONIC CYLINDRICAL CAVITY NOISE GENERATION

Marco Grottaurea<sup>1\*</sup>, Aldo Rona<sup>1†</sup>

<sup>1</sup>Department of Engineering  
University of Leicester, Leicester, LE1 7RH  
United Kingdom

\*mg165@le.ac.uk

†ar45@le.ac.uk

### Abstract

At typical landing speeds, the cylindrical cavity flow that develops past an aircraft fuel vent displays tonal convective streamwise instabilities. The higher frequency range of the noise radiated by such a cavity compared to flap noise is perceived by a ground observer as louder with respect to what its amplitude in decibel would suggest, due to the dB(A) weighting. A three-dimensional time-dependent numerical model of a cylindrical cavity flow is obtained using an in-house three-dimensional compressible laminar solver. This simulation predicts the flow instability and gives a preliminary understanding of the influence of the inflow momentum thickness ( $\theta$ ) on the flow unsteadiness. Time-dependent cavity flow models are obtained at two different Reynolds numbers ( $Re_\theta$ ) based on the inflow momentum thickness,  $Re_\theta = 8850$  and  $Re_\theta = 10750$ , for two diameter to depth ratios ( $L/D$ ), 0.71 and 2.5. The near-field sound pressure level (SPL), the pressure coefficient  $C_p$ , and the shear layer spanning the cavity are analyzed. The numerical experiments suggest that the deep cavity is characterized by a self-sustained instability and that the shallow cavity is characterized by a steady flow recirculation. The near-field SPL was compared with past Euler predictions to study the influence of the shear layer growth on the radiating pressure field. In the laminar predictions, it was found that the amplitude of the outgoing pressure waves is lower, due to a weaker interaction of the open cavity shear-layer with the downstream solid edge.

### 1. INTRODUCTION

High by-pass ratio turbofans and recent advances in aircraft engine technology have significantly reduced the overall engine noise with respect to 1960's aircraft. Therefore other noise sources, such as the high lift system and the undercarriage, have become more prominent, especially during landing. Noise restrictions imposed on aircraft operators have been reducing the Effective Perceived Noise Level (EPNL) by 20 dB every twenty years, so that now the noise

from other airframe recesses, such as the fuel vents, have become of interest to reach further reductions in the landing noise foot-print. The lower intensity noise emission from fuel vents as compared to high-lift devices can become significant in the EPNL by the dB(A) weighting of the higher frequency noise that characterizes these recesses. In this study, a cylindrical cavity is considered as a low fidelity model for a wide-body civil aircraft fuel vent. In the literature, cylindrical cavity flows have been more sparingly studied with respect to rectangular ones, therefore the present study adds to the available literature.

Powerful computational platforms and code parallelization allow the computational modelling of representative industrial geometries by conventional Computational Fluid Dynamics[1]. Advances in high-order low dissipation and dispersion schemes have lowered the cost of aeroacoustic models to a more affordable level, so that some geometries of industrial interest can now be tackled. Still, the large computational domain size required to resolve the near-field acoustic propagation and the use of acoustic absorbing inflow and outflow boundary conditions significantly limit the range of geometries that can be investigated by aeroacoustic models[2]. Past cavity aeroacoustic investigations mainly focussed on rectangular enclosures, due to the savings in computer time that can be achieved by the use of a Cartesian mesh. The computational resources now available enable the use of a curvilinear conformal mesh to tackle a cylindrical cavity[3, 4].

In a typical open cavity flow[5], once the oncoming boundary layer reaches the enclosure leading edge, eddies are shed due to the sharp edge and these are convectively amplified towards the cavity trailing edge. The interaction between the trailing edge and the vortices produces pressure waves scattered with a broad directivity[6]. Part of these waves escapes the cavity and is perceived in the far-field as noise and part is reflected upstream. The latter reflection interacts with the incoming boundary layer flow at the cavity leading edge, driving the shedding of new vortices. This feedback process was first observed and described by Rossiter[7]. According to the simple model for rectangular cavity flows of Rowley et al.[8], this instability mechanism can either be self-sustained or lightly damped, depending on the inflow conditions and the geometry.

To obtain a preliminary understanding of this instability mechanism and the effect of viscosity on the flow pattern, a laminar solver is used in this study. The predictions are compared with those from an Euler model[9] in which the incoming boundary layer thickness is unresolved. Whereas the feedback instability mechanism can be captured with an Euler simulation, the shear layer growth towards the cavity trailing edge cannot. In the inviscid simulation, the shear layer is modelled as a vortex sheet and its streamwise growth is essentially zero, whereas it thickens if a dissipative term due to viscosity is added to the governing equations.

## 2. CYLINDRICAL CAVITY FLOW MODEL

### 2.1. Test case description

The following dimensional variables characterize the cavity flow[10]: the streamwise length ( $L$ ), the span ( $W$ ), the depth ( $D$ ), the free stream velocity ( $U_\infty$ ), the leading edge boundary layer momentum thickness ( $\theta$ ), the speed of sound ( $a_\infty$ ) and the kinematic viscosity ( $\nu_\infty$ ). These can be rearranged into the corresponding non-dimensional parameters:  $L/D$ ,  $L/\theta$ ,  $M_\infty = U_\infty/a_\infty$ , and  $Re_\theta = U_\infty\theta/\nu_\infty$ .

A low fidelity aircraft fuel vent model consists of a cylindrical cavity placed one metre down-

stream of the leading edge of a flat plate, and  $L$  and  $W$  are equal to the cylinder diameter. Two different diameter to cavity depth ratios are modelled;  $L/D = 2.5$  and  $L/D = 0.71$ , to resolve the changes in the fuel vent pattern associated to the cavity depth at the given test conditions.

To account for the influence of the incoming boundary layer thickness on the cavity flow instability, two different  $Re_\theta$  are selected,  $Re_\theta = 8850$  and  $Re_\theta = 10750$ . The remaining two non-dimensional quantities,  $L/\theta$  and the Mach number  $M_\infty$ , are selected in the simulation as  $L/\theta = 65$  at  $M_\infty = 0.3$ , and  $L/\theta = 62$  at  $M_\infty = 0.235$ .

Over the selected range of non-dimensional parameters ( $L/D, L/\theta, Re_\theta, M_\infty$ ), the cavity flow is open[5] and it is characterized by a major recirculation zone within the cavity and by an unsteady stagnation point on the downstream cavity wall.

## 2.2. Governing equations

The time-dependent Navier-Stokes equations for an inert adiabatic flow under no external force are:

$$\frac{\partial}{\partial t} \mathbf{U} + \nabla \cdot \mathbf{F} = \nabla \cdot \mathbf{F}_v \quad (1)$$

The left hand side of equation (1) contains the conservative variables  $\mathbf{U} = [\rho, \rho \mathbf{u}, \rho e]^T$  and the inviscid fluxes  $\mathbf{F} = [\rho \mathbf{u}, \rho \mathbf{u} \mathbf{u} + p \mathbf{I}, \rho \mathbf{u} (e + p/\rho)]^T$ .  $\rho$  is the flow density,  $p$  the pressure,  $\mathbf{u} = [u, v, w]^T$  the velocity vector,  $e$  the total energy per unit mass,  $\mathbf{I}$  the identity matrix and superscript T denotes the transpose operator. The right hand side is the viscous fluxes vector  $\mathbf{F}_v = [0, \underline{\tau}, \underline{\tau} \cdot \mathbf{u} + k \nabla T]^T$ . The viscous stress tensor  $\underline{\tau} = \mu (\nabla \mathbf{u} + \mathbf{u} \nabla - 2/3 \mathbf{I} \nabla \cdot \mathbf{u})$ ,  $\mu$  is the dynamic viscosity,  $k$  the thermal conductivity and  $T$  the absolute temperature. If  $\mathbf{F}_v = 0$ , equation (1) becomes the Euler equations.

## 2.3. Computational mesh

A conformal curvilinear mesh is used to model the cylindrical cavity. By multi-zone decomposition, the flow domain has been divided into six zones, as shown in figure 1(a). Each zone has a similar number of cells to even out the computational load among the processors.

The domain outside the cavity is  $18.4 L \times 18.4 L \times 9.6 L$ . A large domain of the order of  $20 L$  is used to resolve at least one full acoustic wavelength of the radiating sound. The selected computational domain volume is the smallest that prevents the non-linear interaction of the acoustic radiation in the computational domain with the potential flow at the outer domain boundaries[11]. The stretching ratio is roughly constant in all the domain and is 1.05. 13 and 14 cells are used to discretize the inflow boundary layer in the wall-normal direction at  $Re_\theta = 10750$  and  $Re_\theta = 8850$  respectively. 0.34 million cells are used in the  $L/D = 0.71$  cavity model and 0.327 million cells in the  $L/D = 2.5$  model.

The cell skewness ( $\gamma_1$ ) in any  $z \geq 0$  plane, shown in figure 1(b), is:

$$\gamma_1 = \frac{\max(\|\mathbf{d}_1\|, \|\mathbf{d}_2\|)}{\min(\|\mathbf{d}_1\|, \|\mathbf{d}_2\|)} - 1 \quad (2)$$

In equation (2),  $\mathbf{d}_1$  and  $\mathbf{d}_2$  are the diagonals of the lower face of computational cell  $i, j, k$  and are:  $\mathbf{d}_1 = \mathbf{x}_{i+1, j+1} - \mathbf{x}_{i, j}$  and  $\mathbf{d}_2 = \mathbf{x}_{i, j+1} - \mathbf{x}_{i+1, j}$ , where  $\mathbf{x}_{i, j}$ ,  $\mathbf{x}_{i+1, j}$ ,  $\mathbf{x}_{i, j+1}$ ,  $\mathbf{x}_{i+1, j+1}$  are the

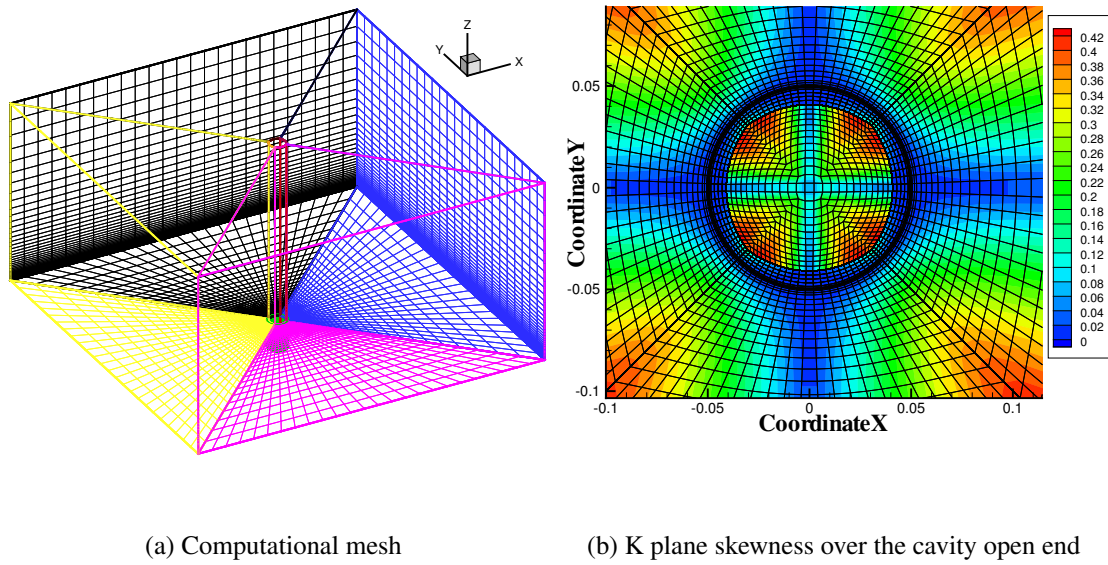


Figure 1. Computational domain details

position vectors of the face vertices.

The four corners of the central zone, in red in figure 1(a), is where the skewness has the maximum value of 0.42. As the skewness is an index of the local mesh deformation, it is best minimized throughout the domain. An advantage of the generated computational mesh is the modest deformation of the cells around the perimeter of the cylinder. The skewness at these positions is close to 0, which helps to resolve the growing boundary layer around the cylindrical wall.

#### 2.4. Inflow conditions

The inflow to the computational domain is imposed by solving the compressible non-dimensional form of the Blasius equation for a laminar boundary layer. The following equations describe the flow field[12]:

$$f'''(\eta) + f(\eta)f''(\eta) = 0 \quad (3)$$

$$\frac{T_{aw}}{T_\infty} = 1 + \frac{\gamma - 1}{2} r M_\infty^2 \quad (4)$$

Equation (3) is the non-dimensional Blasius equation for a laminar boundary layer, where  $\eta = y\sqrt{\frac{U_\infty}{2\nu x}}$  and  $u = U_\infty f'(\eta)$ . Equation (4) gives the adiabatic wall temperature. In this,  $r$  is the recovery factor and  $\gamma$  the specific heats ratio. For a Prandtl number ( $Pr$ ) in the range  $0.1 < Pr < 3$ , the recovery factor is  $r = \sqrt{Pr}$ .

From equations (3) and (4) and assuming the static pressure  $p$  is constant across the boundary layer, the conservative variables distribution is known as a continuous function of the flow-normal direction ( $z$ ). The discretized conservative variables vector distribution  $\mathbf{U}_i$  is the average of the local value of  $\mathbf{U}$  over the cell:

$$\mathbf{U}_i = \frac{1}{\Delta z} \int_{z_i}^{z_{i+1}} \mathbf{U}(\tilde{z}) d\tilde{z} \quad (5)$$

In the equation (5), it is assumed that the local variation of  $\mathbf{U}$  in the flow-normal direction ( $z$ ) is larger compared to that in the streamwise direction ( $x$ ) and in the spanwise direction ( $y$ ).

## 2.5. Boundary condition sensitivity analysis

Robust and accurate Non-Reflective Boundary Condition (NRBC) are crucial in computational aeroacoustic applications[13]. Giles[14] gives a variety of non-reflective boundary conditions for one-dimensional and two-dimensional supersonic flows. Based on these, a three-dimensional extension by Manna[15] is used in this study. To evaluate the sensitivity of the numerical solution with respect to these boundary conditions, the near-field sound pressure level (SPL) is examined. To compute the SPL, 25 frames describing a full period of oscillation were used. Figure 2 shows a monotonic reduction of the SPL from the enclosure towards the computational domain through-flow boundaries. This indicates that the boundary conditions allow the passage of the outgoing pressure waves with no appreciable reflection.

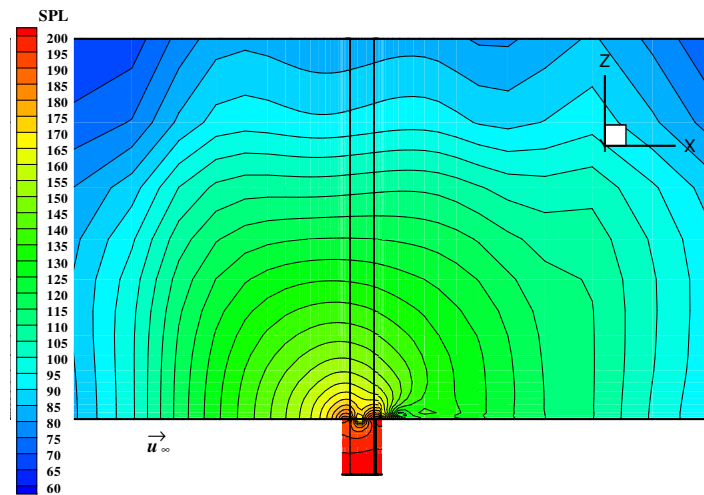
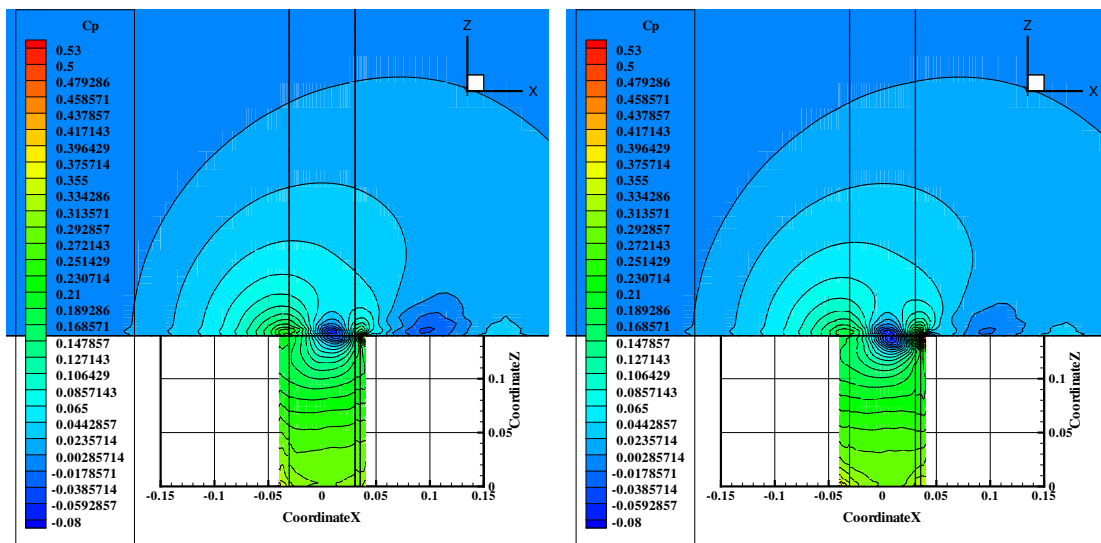


Figure 2. Near-field SPL on the  $y = 0$  plane.  $SPL_{min} = 60 \text{ dB re } 20 \mu Pa$ ,  $SPL_{max} = 200 \text{ dB re } 20 \mu Pa$ .

## 3. LAMINAR SIMULATION RESULTS

In the Euler simulation[9], it was found that  $L/D$  influences the development of the unsteady vortex structure within the cavity. This is also the case for the laminar simulation. Figures 3(a) and 3(b) show a pressure coefficient ( $C_p$ ) iso-contours snapshot from the laminar cavity model with  $L/D = 0.71$  during a mass ejection sequence. The prediction is characterized by an asymmetric vortex structure with respect to the  $y = 0$  plane, as shown by the different streamwise position of the  $C_p$  maxima along the cavity shear layer in figures 3(a) and 3(b). Vortices alternatively impinge on the right and on the left side of cavity trailing edge, producing a three-dimensional mass impingement and ejection sequence. Their interaction with the solid edge produces pressure waves. An asymmetric vortex structure has been found by Hering et al.[4, 16] in their experimental work on a  $L/D = 2$  incompressible cylindrical cavity flow at  $M_\infty = 0.08$ . The  $L/D = 2.5$  shallow cavity predictions are shown in figures 4(a) and 4(b). The flow model



(a)  $C_p$  on the  $y = -0.3L$  plane,  $L/D = 0.71$ .  
 $C_{p_{max}} = 0.376$

(b)  $C_p$  on the  $y = 0.3L$  plane,  $L/D = 0.71$ .  
 $C_{p_{max}} = 0.53$

Figure 3. Pressure coefficient during mass ejection.  $C_p = (p - p_\infty)/(1/2\rho U_\infty^2)$ .

is steady, indicating that the laminar cavity is behaving as a lightly damped system at these conditions. A mesh refinement of 50% was used to check whether the steady flow was the result of the mesh-related numerical viscosity, since the Euler model[9] of the same cavity predict a self-sustained instability. Although the refined mesh simulation better resolves the symmetric recirculation within the cavity, it also gives a steady flow, as shown in figure 4(b).

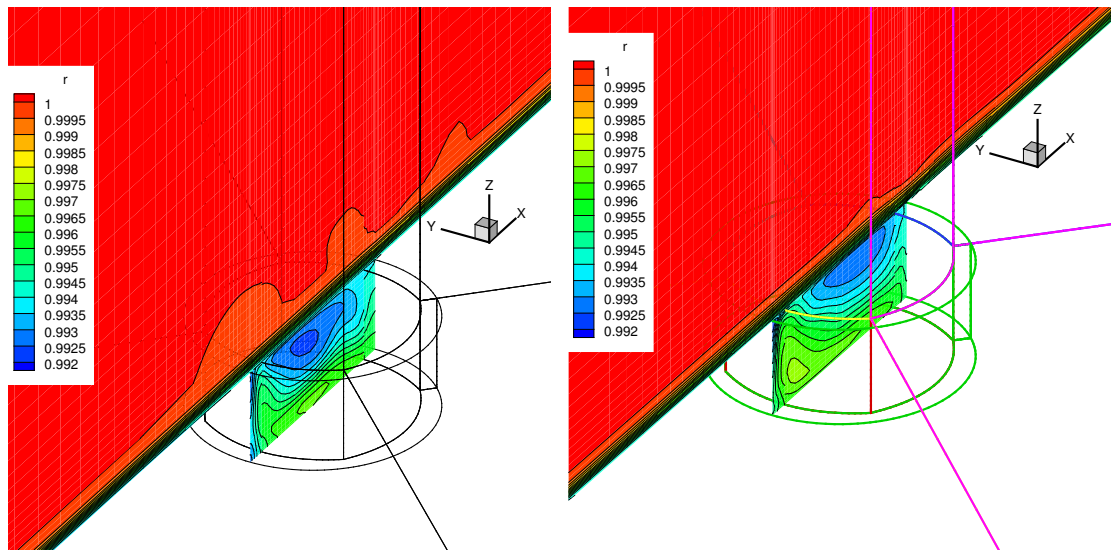
As the shear layer thickens across the cavity opening, in figure 5, its interaction with the cavity trailing edge is weaker with respect to the vortex-edge interaction in the Euler model[9]. In the laminar simulations, the SPL at  $(x, y, z) = (0.5L, 0, 8L)$  is reduced by 3 dB for  $L/\theta = 65$  and by 22 dB for  $L/\theta = 62$ .

#### 4. CONCLUSION

Shallow and deep cylindrical cavity flows were modelled at different inflow conditions. The results suggest that the flow instability amplitude from the shallow cavity configuration is lower with respect to the deep cavity one, possibly due to the proximity of the floor preventing the onset of the azimuthal instability modes in the enclosure. However, the frequency of the radiated noise from the  $L/D = 2.5$  shallow cavity is higher than at  $L/D = 0.71$ [9]. Therefore the EPNL from a shallow aircraft fuel vent may be perceived as louder due to the dB(A) weighting. This numerical experiment has also shown that the inflow boundary layer thickness has a significant effect on the SPL, as in a rectangular cavity.

#### 5. ACKNOWLEDGEMENT

This research project has been supported by a Marie Curie Early Stage Research Training Fellowship of the European Community's Sixth Framework Programme under contract number



(a) 0.31 million cells baseline mesh

(b) 50% refined mesh in the cavity

Figure 4. Dimensionless  $\rho/\rho_\infty$  iso-contours on the  $y = 0$  plane

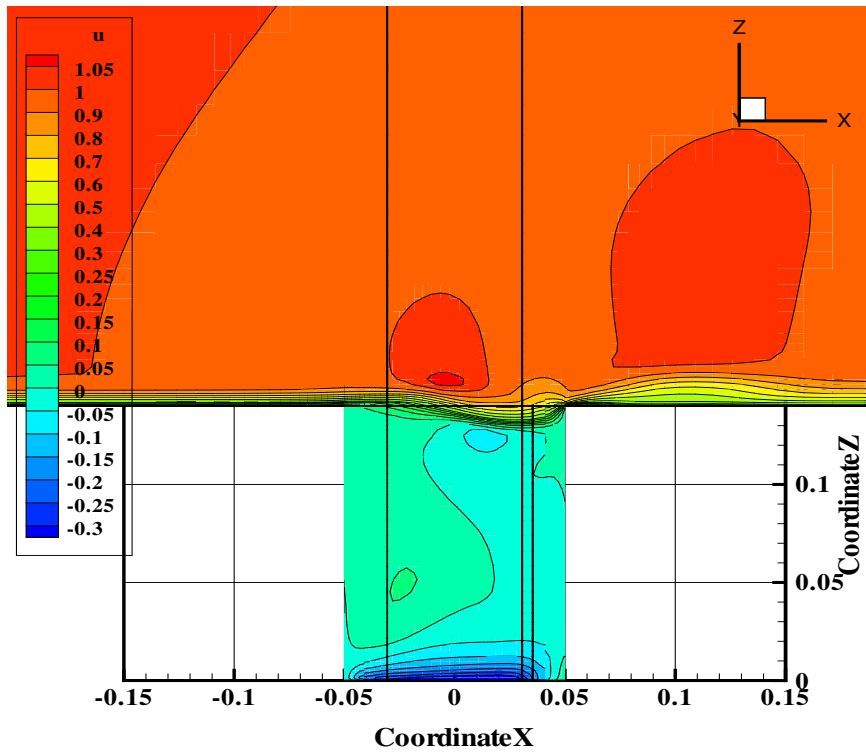


Figure 5. Dimensionless streamwise velocity on the  $y = 0$  plane

MEST CT 2005 020301.

## REFERENCES

- [1] L. Long, P. Morris, and A. Agarwal, “A review of parallel computing in computational aeroacoustics,” *Int. J. Computational Fluid Dynamics*, vol. 18, no. 6, pp. 493–502, 2004.
- [2] D. G. Crighton, “Boundary conditions for direct computation of aerodynamic sound generation,” *Progress in Aerospace Sciences*, vol. 6, no. 1, pp. 31–96, 1975.
- [3] A. V. Bunyakin, “Laminar boundary layer in a flow past an aerofoil with a circular cavity,” *Fluid Dynamics*, vol. 33, no. 2, pp. 196–200, 1998.
- [4] T. Hering, J. Dybenko, and E. Savory, “Experimental verification of CFD modeling of turbulent flow over circular cavities,” in *Canadian Society of Mechanical Engineering Forum*, Kananaskis, Canada, May 2006.
- [5] A. Charwat, J. Roos, F. Dewey, and J. Hitz, “An investigation of separated flows. Part I: The pressure field,” *J. Aerospace Sci.*, vol. 28, no. 6, pp. 457–70, 1961.
- [6] A. Powell, “Theory of vortex sound,” *J. Acoustical Society of America*, vol. 36, no. 1, pp. 177–95, 1964.
- [7] J. Rossiter, “Wind-tunnel experiments on the flow over rectangular cavities at subsonic and transonic speeds,” Aeronautical Research Council Reports and Memoranda, Technical Report 3438, 1964.
- [8] C. Rowley, D. Williams, T. Colonius, R. Murray, D. MacMartin, and D. Fabris, “An analysis of the discontinuous Galerkin method for wave propagation problems,” *J. Computational Physics*, vol. 151, pp. 921–946, 1999.
- [9] M. Grottaure and A. Rona, “Noise sources from a cylindrical cavity,” 13th AIAA/CEAS Aeroacoustics Conference, Rome, Italy, Tech. Rep. 2007-3723, 2007.
- [10] T. Colonius, “An overview of simulation, modeling, and active control of flow/acoustic resonance in open cavities,” *Progress on Aerospace Sciences*, vol. 40, pp. 365–416, 2001.
- [11] T. Colonius and S. Lele, “Computational aeroacoustics: progress on nonlinear problems of sound generation,” *Progress on Aerospace Sciences*, vol. 40, pp. 365–416, 2004.
- [12] F. White, *Viscous fluid flow*, 2nd ed. McGraw-Hill Series in Mechanical Engineering, 1991.
- [13] F. Hu, “Absorbing boundary conditions,” *Int. J. Computational Fluid Dynamics*, vol. 18, no. 6, pp. 513–22, 2004.
- [14] M. Giles, “Non-reflecting boundary conditions for euler equation calculation,” *AIAA J.*, vol. 28, no. 12, pp. 2050–58, 1990.
- [15] M. Manna, “A three dimensional high resolution compressible flow solver,” PhD thesis, Faculty of Applied Science, Université Catholique de Louvain, October 1992.
- [16] J. Dybenko, T. Hering, and E. Savory, “Turbulent flow over circular cylindrical cavities with varying depth to diameter ratio,” in *International Council of the Aeronautical Sciences Congress*, Hamburg, Germany, September 2006.